Life Sciences 231 (2019) 116545

Contents lists available at ScienceDirect

Life Sciences

journal homepage: www.elsevier.com/locate/lifescie

Enhanced penetration and cytotoxicity of metformin and collagenase conjugated gold nanoparticles in breast cancer spheroids

Elaheh Dalir Abdolahinia[a,b], Samad Nadri[c,*], Reza Rahbarghazi[d], Jaleh Barar[b,e], Ayoub Aghanejad[b], Yadollah Omidi[b,e,**]

[a] Department of Medical Biotechnology, Zanjan University of Medical Sciences, Zanjan, Iran
[b] Research Center for Pharmaceutical Nanotechnology, Biomedicine Institute, Tabriz University of Medical Sciences, Tabriz, Iran
[c] Department of Medical Nanotechnology, Zanjan University of Medical Sciences, Zanjan, Iran
[d] Department of Applied Cell Sciences, Faculty of Advanced Medical Sciences, Tabriz University of Medical Sciences, Tabriz, Iran
[e] Department of Pharmaceutics, Faculty of Pharmacy, Tabriz University of Medical Sciences, Tabriz, Iran

ARTICLE INFO

Keywords:
Cancer stem cells
Collagenase
Gold nanoparticles
Mammospheres
Metformin
Nanomedicine

ABSTRACT

Aims: The extracellular matrix (ECM) within the tumor nest plays a key role in cancer cell proliferation and invasion. It has been proven that the increased density of ECM, especially collagen network, correlates with the poor distribution of gold-nanoparticles (GNPs) to the tumor mass. Here, for the first time, we examined the combined effect of collagenase (COL) with metformin (MET)-conjugated GNPs on mammosphere generated from JIMT-1 breast cell line in vitro.

Main methods: Mammospheres (on days 7 and 14) and monolayer culture were treated with MET, MET-GNPs, and a mixture of COL-GNPs and MET-GNPs for 5 days. To assess the impacts of the engineered nanoparticles (NPs) on the survival/apoptosis of cancer cells and cancer stem cells (CSCs), the amount/activity of collagen and the expression of pyruvate kinase M2, different methods were applied, including MTT, flow cytometry, immunofluorescence, ELISA and real-time PCR analyses. Our results confirmed the enhanced cytotoxic effects of MET-GNPs combined with COL-GNPs on mammospheres compared to the cells treated with MET alone or MET-GNPs.

Key findings: Upon treatment with the mixture of MET-GNPs and COL-GNPs, the population of the apoptotic cells was significantly increased. A marked reduction was found in the number of $CD24^{-}/CD44^{+}$ CSCs and the amount of collagen in the group received a mixture of MET-GNPs and COL-GNPs.

Significance: Based on our findings, the use of COL can improve the cellular interaction/penetration of MET-GNPs in mammospheres and its antitumor impacts on the CSCs.

1. Introduction

Most of the preclinical examinations are commonly performed using two-dimensional (2D) in vitro condition for the development and validation of novel anti-cancer agents. However, such systems have been criticized for the lack of the cell–to–cell intercommunication, the paucity in the extracellular matrix (ECM)-mediated signaling and the formation of a relevant microenvironment [1,2]. By providing a three-dimensional (3D) condition as a spheroid/organoid model, intercellular and extracellular digitation among cells might occur much better than the 2D culture. Therefore, in vitro 3D systems seem to serve as a suitable tool, which may not show the limitations associated with the 2D systems [3]. In the case of solid tumors, a spheroid (the so-called tumoroid) provides hypoxic areas with a central necrotic zone after reaching to 500 μm in diameter, representing additional important hallmarks of solid tumors [4].

The formation of the tumor microenvironment (TME) in solid tumors is a well-documented phenomenon, which facilitates cancer progression and invasion [5–8]. In the TME, the distribution pattern of drug molecules in the outer (normoxic area) and inner (hypoxic area) sites of the tumor mass appears to be uneven, in large part because of the remodeling of the ECM and the presence of highly pressurized tumor interstitial fluid [9–11]. Seemingly, within the TME, the hypoxic layer leads to the upregulation of some genes that might reinforce the transition of cancer epithelial cells to a much more malignant phenotype of cancer cells, the so-called cancer stem cells (CSCs). Metformin

* Corresponding author.
** Correspondence to: Y. Omidi, Research Center for Pharmaceutical Nanotechnology, Biomedicine Institute, Tabriz University of Medical Sciences, Tabriz, Iran.
E-mail addresses: nadri_s@zums.ac.ir (S. Nadri), yomidi@tbzmed.ac.ir (Y. Omidi).

https://doi.org/10.1016/j.lfs.2019.116545
Received 6 April 2019; Received in revised form 5 June 2019; Accepted 5 June 2019
Available online 07 June 2019
0024-3205/

(MET), a first-line drug for the treatment of diabetes, is proven to play an important role in suppressing the CSCs in solid tumors such as breast cancer niches [12–15]. The direct cytotoxic effect of MET has previously been shown on cancer cells, mainly through the suppression of pyruvate kinase isozymes M2 (PKM2) expression. PKM2 is a key player in the modulation of the aerobic glycolytic pathway (so-called the Warburg effect) in embryonic tissues and solid tumors [16]. This enzyme was shown to associate with the tumorigenesis and cancer cell resistance through both AMP-activated protein kinase (AMPK)-dependent and independent mechanisms under the hypoxic condition [17]. Furthermore, PKM2 can modulate the epithelial-mesenchymal transition (EMT) of cancer cells [18], increase the CSCs under hypoxia [19], and promote the tumor angiogenesis through interacting with Oct-4 [20], HIF-1α [21], STAT3 [22], and β-catenin [23] and stimulating transcriptional activities.

Compelling evidence has revealed that drug diffusion into tumor mass might decrease with an increase in the collagen content in the ECM. As a result, only a low amount of administered drug molecules might reach to the inner area of the solid tumor where the CSCs are accommodated [24]. Thus, after the first course of the treatment, the untouched CSCs can trigger the relapse of the disease. It has been reported that the breast cancer niche is 10 times denser than the normal tissue [25,26]. This condition can promote the emergence and/or maintenance of CSCs inside the tumor niche, and favor their survival, metastasis, and migration.

Commensurate with these descriptions, strategies for improving drug penetration into solid tumors continue to be largely demanded. In some experiments, it was found that the degradation of collagen using collagenase (COL) may be considered as an effective strategy to enhance the biodistribution of drugs into the inner area of the tumor [27]. The conjugation of COL to the gold nanoparticles (GNPs), which is a non-toxic nanocarrier, was shown to enhance the capacity of drug penetration [28].

In the current experiment, we aimed to develop the three-dimensional culture of JIMT-1 breast cell-line using the hanging-drop method to simulate in vivo situation such as cell to cell contacts and cell to ECM interactions. We investigated whether mammosphere can provide a 3D model which enrich the growth of rare cell types such as CSCs to examine the suppressing action of MET against CSCs. In addition, the effects of ECM network were examined in terms of resistance to penetration of GNPs, which may contribute to the decline of drug efficacy. Therefore, we worked on enhancing the eradication of the CSCs using conjugation of MET and COL to the GNPs to improve drug penetration rate and therapeutic outcomes.

2. Material and methods

2.1. Cell culture protocol

Human breast cancer JIMT-1 cell line (from Pasteur Institute, National Cell Bank of Iran) was expanded in Dulbecco's Modified Eagle Medium: Nutrient Mixture F-12 (DMEM-F12) supplemented with 10% fetal bovine serum (FBS) and 1% penicillin-streptomycin. The cells were maintained in a humidified atmosphere at 37 °C with 5% CO_2. For the subculture of cells, we used 0.25% Trypsin-EDTA. Cells between passages 3–6 at 80% confluence were used for subsequent analyses. All materials for the culture medium were purchased from Gibco (Thermo Fisher Scientific, Waltham, USA).

2.2. Mammosphere culture

Mammosphere was generated employing the hanging drop method as previously described [29]. For this mean, cells at the initial number of 400 were mixed with 25 μL of medium containing 25% METHOCEL™ (Sigma, St. Louis, Missouri, USA) and 10% FBS and carefully placed under the lids of cell culture plate and incubated for a period of 7 to 14 days.

2.3. Experimental procedure

2.3.1. Synthesis of gold nanoparticles (GNPs)

GNPs synthesis was performed through a modified Stucky method [30]. Briefly, $HAuCl_4{\cdot}3H_2O$ (1 mM) was added to the mixture of 10 mL of tetraline banzan and 10 mL of oleylamine at 4 °C and gently stirred. Then, a reducing solution containing *tert*-butylamine borane complex (TBAB) (1 mM), tetraline banzan (1 mL) and oleylamine (1 mL) were injected to the prepared mixture at 4 °C till a red color appeared. Then, GNPs were washed (×3) using 15 mL of acetone, collected by centrifugation (4000 ×*g*, 5 min), and redispersed in *n*-hexane. The GNPs were modified using 11-mercaptoundecanoic acid (MUA). For this purpose, MUA (0.2 g) was dissolved in 20 mL of chloroform and added to GNPs solution while stirring. The mixture was allowed to react at room temperature overnight. Thereafter, MUA-GNPs were precipitated through centrifugation (4000 ×*g*, 10 min).

2.3.2. Production of metformin (MET)-conjugated GNPs

To synthesize MET-GNPs, the MET-HCL (1.4 mM) (Alborz-Bulk Pharmaceutical Company; Tehran, Iran) was added to dimethyl sulfoxide (DMSO, Merck, Darmstadt, Germany) solution containing 0.1 *g* of the modified MUA-GNPs in the presence of N,N′-dicyclohexylcarbodiimide (DCC) (0.8 mM) and N-hydroxysuccinimide (NHS) (0.8 mM). To eliminate HCl, triethylamine substrate was added, and the mixture stirred gently to form an amide bond. After 24 h, the solution was centrifuged at 4000 ×*g* for 5 min to precipitate the MET-GNPs.

2.3.3. Production of collagenase (COL)-conjugated GNPs

For this propose, 335.3 μL of 100 mg/mL *Clostridium Histolyticum* origin COL (Sigma-Aldrich, St. Louis, USA), DCC (0.8 mM) and NHS (0.8 mM) were dissolved in phosphate buffered saline (PBS) solution. Thereafter, an equal volume of the modified MUA-GNPs was introduced to the enzyme solution and allowed to react overnight at room temperature to create an amide bond. COL-MUA-GNPs conjugate was harvested by centrifuging at 4000 ×*g* for 5 min. To generate total MET-GNPs and COL-GNPs composition, COL-MUA-GNPs and MET-MUA-GNPs were mixed (1–10% w/w). The enzymatic activity of COL conjugated to GNPs was determined using a colorimetric Collagenase Activity Assay Kit (Abcam, Cambridge, UK).

2.3.4. Characterization of conjugated GNPs

To determine the conjugating of MET and COL with GNPs, FTIR spectroscopy (Vertex 70, Bruker, Hamburg, Germany) was performed. Thus, freeze-dried samples were mixed with potassium bromide (KBr) to form the standard disks and the FTIR spectra were recorded from 400 to 4000 cm^{-1}. Also, the net charge and size of the particles were measured using dynamic light scattering (DLS) using a Microtrac particle analyzer (Nanotrac Wave II Q, Krefeld, Germany) and transmission electron microscopy (Carl Zeiss, Oberkochen, Germany) as previously described [31].

2.3.5. Analysis of collagenase activity

Collagenase activity was determined by means of a Collagenase Activity Assay Kit, following the manufacturer's instructions (Abcam, Cambridge, UK), using 0.1 and 1 mg/mL of COL-GNPs. The activity of the enzyme in the solution was determined by measuring the absorbance of each sample using Synergy HTX plate reader (BioTek Instruments, Inc., Winooski, USA) and compared to the equivalent concentration of free COL and GNPs alone as the negative control. The assay was performed for a period of 5 days to confirm the stability of the enzymatic activity.

2.3.6. Analysis of GNPs penetration in mammospheres

To determine the penetration rate, the accumulation of a designated

amount of COL-GNPs in spheroid was measured based on changes in collagen content by means of indirect ELISA. First, proteins were extracted by pepsin (0.1 mg in 0.5 M acetic acid) at 4 °C from the control, COL (0.1 and 1 mg/mL), GNPs, and COL-GNPs. Then, proteinase activity was inhibited by adding anti-protease cocktail, including 1, 10-phenanthroline (2 mM) and phenylmethylsulfonyl fluoride (PMSF) (2 mM). For the ELISA experiment, a 96-well microplate was coated with 1 μg/mL of extracted protein per well and incubated at 4 °C overnight. After washing (× 3), the wells were blocked with 100 mL of 2% bovine serum albumin (BSA) (Sigma-Aldrich Corp., St. Louis, USA) in PBS and incubated for 2 h at 37 °C. The wells were then washed several times with PBS and 1 μg anti-collagens I to V antibody (Abcam, Cambridge, UK) was added per well and incubated at 37 °C for 1 h. Following washing, 1 μg/well of AlexaFluor-488 labeled goat anti-rabbit IgG (Abcam, Cambridge, UK) was used and incubated at 37 °C for 30 min. Finally, the plate was subjected to Cytation™ 5 imaging reader at 488 nm (BioTek Instruments, Inc., Winooski, USA) and the collagen content of each sample was determined by comparison to the standard curve.

2.4. In vitro cytotoxicity assay

In the current experiment, the treated JIMT-1 cells were classified into six groups as follows: (I) control, (II) GNPs alone, (III) MET alone, (IV) MET-GNPs, (V) COL-GNPs (collagenase concentration equal to 0.1 and 1 mg/mL), and (VI) mixture of COL-GNPs and MET-GNPs. The cell survival rate was determined by means of the MTT assay.

For the conventional 2D culture expansion, the cells were cultured at a density of 3.0×10^3 cells/well in a 96-well plate. In 3D culture system, 7- and 14- day old spheroids were transferred into the uncoated v-bottom 96 well plates. The next day, cells were incubated with the designated concentrations of drug compounds. On day 5, about 200 μL of 5 mg/mL MTT (Sigma, St. Louis, USA) was added to each well and kept at 37 °C for 4 h. Following the removal of supernatants, 100 μL of DMSO was added to each well and shaken. Each sample absorbance was read at 570 nm using a multi-well plate reader, ELx808 (Biotek Instruments, Winooski, USA). In the current experiment, the cell-culture media was not changed during the entire period of the treatment. Further, the multicellular resistance index (MCRI), which represents the ratio of the IC_{50} in mammosphere to the IC_{50} in monolayer, was measured.

2.5. Detection of collagen content in JIMT-1 mammospheres

To confirm the efficiency of synthesized nanopartilces (NPs) harboring drug complex in decomposing mammospheres, the immunofluorescence imaging was performed. Spheroids from different groups were fixed by ice-cooled 4% paraformaldehyde solution for 20 min and permeabilized by blocking buffer (eBiosciences, Thermo Fisher Scientific, Waltham, USA) for 10 min. Thereafter, the cells were incubated with polyclonal rabbit anti-human collagen cocktail including anti-collagens I to V overnight at 4 °C. After three times washing with PBS (each for 10 min), incubation with AlexaFluor-488 labeled goat anti-rabbit IgG was performed, also 1μg/mL DAPI (Sigma, St. Louis, USA) was used for counterstaining. Finally, spheroids were visualized by Cytation ™ 5 imaging reader (BioTek Instruments, Inc., Winooski, USA).

2.6. $CD44^+/CD24^-$ cells immunophenotyping

To evaluate the population of the cancer stem cells (CSCs), we used flow cytometry analysis. All cells growing in different conditions were washed with PBS solution, and then, Accutase® was used for the cell detachment and generation of the single cell suspension. For the immunophenotyping of the CSCs, a panel of antibodies was used, including FITC-conjugated anti-CD44 (eBiosciences, Thermo Fisher Scientific, Waltham, USA) and PE-conjugated anti-CD24 antibodies (eBiosciences, Thermo Fisher Scientific, Waltham, USA) with the appropriate isotype controls. In short, samples were incubated with a recommended concentration of antibodies and maintained at 4 °C in the dark for 30–40 min. After washing with PBS, the cells were examined using FACS Calibur flow cytometry (Becton, Dickinson and Co., Franklin Lakes, USA) and data were analyzed by FlowJo software (ver. X10.0.7r2).

2.7. Analysis of apoptosis by Annexin V/PI staining

Single cell suspensions either from 3D or 2D cultures were centrifuged at 300 × *g* for 5 min. After washing with PBS, the cells were exposed to 5 μL FITC-conjugated mouse anti-human annexin-V for 30 min followed by exposure to 10 μL propidium iodide (PI) (eBiosciences, Thermo Fisher Scientific, Waltham, USA) for 10 min. Then, the percentage of the early/late apoptotic and necrotic cells were determined.

2.8. Analysis of pyruvate kinase M2 by real-time PCR

For this propose, total RNA was extracted from 2D cultured cells and 60 mammospheres for each treatment using Trizol® Reagent (Ambion Inc., Life Technologies, Carlsbad, USA) from different groups. The isolated RNA (2 μg) was reverse-transcribed using a cDNA synthesis kit (Fermentas, Waltham, USA). The cDNA (10 ng) was amplified using Power SYBR Green PCR Master Mix (Thermo Scientific, Waltham, USA). Primers were designated by AlleleID ver 7.0 (Table 1). Further, βeta-actin was used for sample normalization as an internal control. Data were analyzed based on the Pfaffl method [32]. Data represent the replicates of at least three sets of separate experiments.

2.9. Statistical analyses

Statistical analyses were carried out using Prism software version 6.0. Data are represented as mean values ± SD. The statistical significance was determined using the One-Way ANOVA followed by Tukey post hoc multiple comparisons test. A p value < 0.05 was considered statistically significant.

Table 1
Primer sequences used for the real-time PCR analysis.

Gene	Accession no	Sequence	Tm (°C)
PKM2	NM_001206797.2	***F*** 5′-GGGTTCGGAGGTTTGATGAAATC-3′ ***R*** 5′-TGAGTAGCACAGATGACAGG-3′	56.8
β-Actin	NM_001101.3	***F*** 5′-TCATGAAGTGTGACGTGGACATCC-3′ ***R*** 5′-AGGAGGAGCAATGATCTTGATCTTC-3′	60

F = forward, R = reverse.

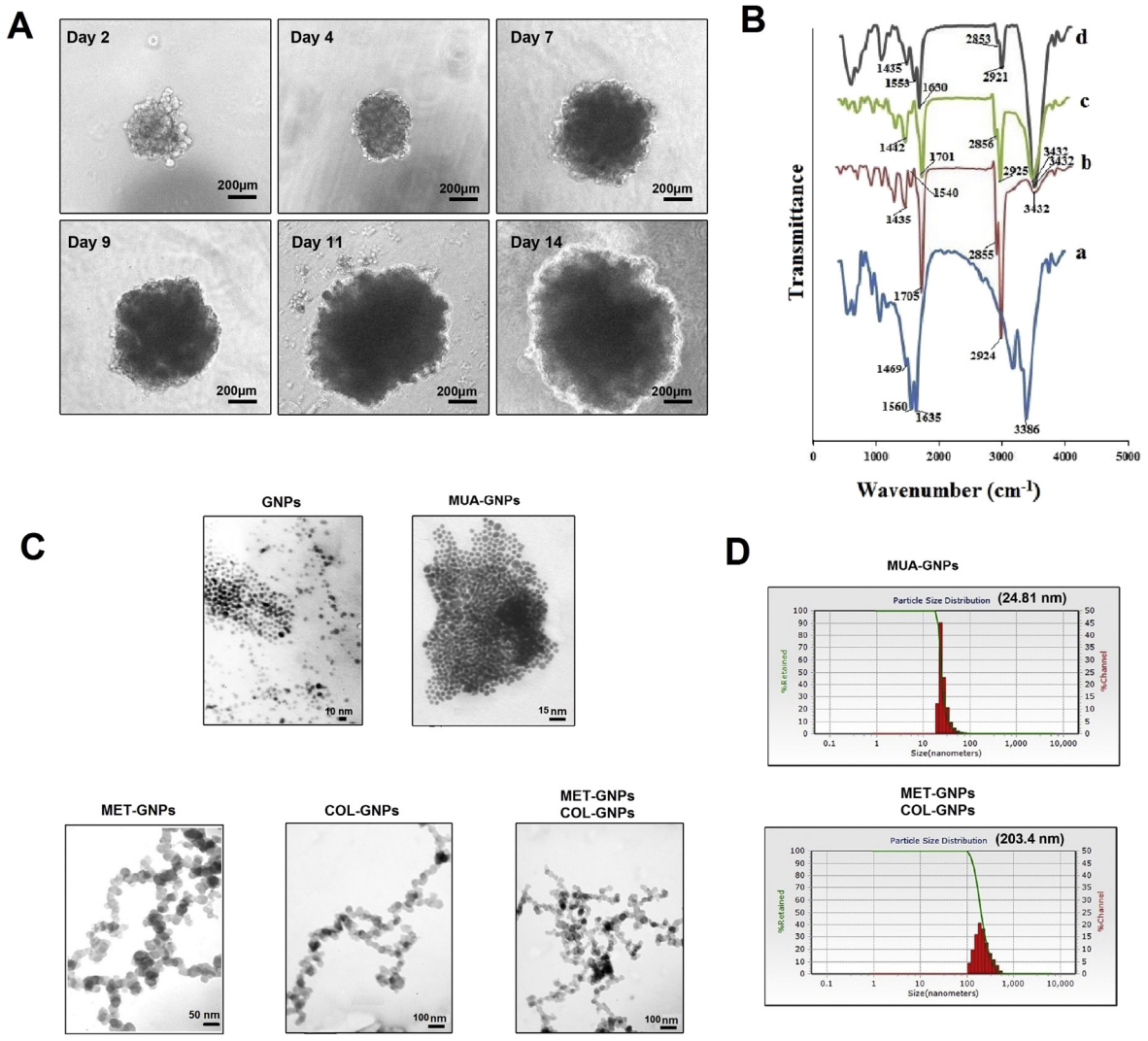

Fig. 1. Morphology of mammospheres and engineered nanoparticles. (A) Formation of mammosphere by hanging-drop method for 14 days. (B) FT-IR analysis of MET-HCL (a), MUA-GNPs (b), COL-GNPs (c), and MET-GNPs and COL-GNPs mixture (d). (C) TEM images of the synthesized GNPs, COL-GNPs and the mixture of MET-GNPs and COL-GNPs. (D) The particle size distribution of MUA-GNPs and the MET-GNPs and COL-GNPs mixture by DLS technique.

3. Results

3.1. Mammosphere growth over a period of 14 days

The hanging drop protocol provides a uniform spheroid microstructure with an approximate diameter of 500 ± 40 and 800 ± 20 μm after 7 and 14 days (Fig. 1A). Based on our experiment, the addition of 25% METHOCEL™, as a crowding agent, led to the aggregation of cells. Several stages of morphological changes were observed during the formation of spheroid prior to the incubation with GNPs. On day 1, several small cell clusters along with individual cells were assembled spontaneously located at the bottom of each drop. On day 7, non-condensed pre-mature spheroids acquired a smooth and continuous surface. After 14 days of spheroid formation, a peripheral highly compact area with a dense cellular network was distinguishable (Fig. 1A).

3.2. Characterization of AuNPs conjugates

The engineered NPs were characterized using FTIR spectroscopy as shown in Fig. 1B. The FTIR spectrum of the MUA-GNPs exhibited the characteristic absorption bands related to stretching vibrations of aliphatic C—H at 2925 and 2856 cm^{-1}, as well as the stretching and bending vibrations of -NH2 and COO^- at 3432 and 1701 cm^{-1}, respectively (Fig. 1B-b). In the spectrum of MET-HCL, the -NH asymmetric stretching and CN stretching vibration occurred at 3386 and 1635 cm^{-1}, respectively (Fig. 1B-a). Moreover, the sharp peaks of COL-GNPs structure were notified at 2924 and 2855 cm^{-1} corresponding to aliphatic compounds (CH) in collagenase backbone (Fig. 1B-c). Finally, the sharp peak of MET-GNPs spectrum appeared at 1630 cm^{-1} indicated the formation of an amide bond between carboxyl groups of MUA and amine group of MET (Fig. 1B-d).

Based on the TEM, the average size of GNPs, MUA-GNPs, COL-GNPs, MET-GNPs, and the COL-GNPs, and MET-GNPs mixture were about 6 ± 0.8, 8 ± 2, 36 ± 4, 33 ± 8, and 49 ± 6 nm, respectively (Fig. 1C). Furthermore, according to DLS analysis, an increase in the diameter was observed for GNPs (25 nm) and the COL-GNPs and MET-GNPs mixture (203 nm) participles (Fig. 1D). The zeta potential (ζ) analysis determined the electrokinetic potential of the GNPs, resulting in improved stability of the samples in the colloidal dispersed state [33]. It was determined that the zeta potential for MUA-GNPs was around −18.3 mV, indicating the presence of free negatively charged carboxylic acid group on the surface of the NPs. The zeta potential of the mixture of COL-GNPs and MET-GNPs was about 20.7 mV.

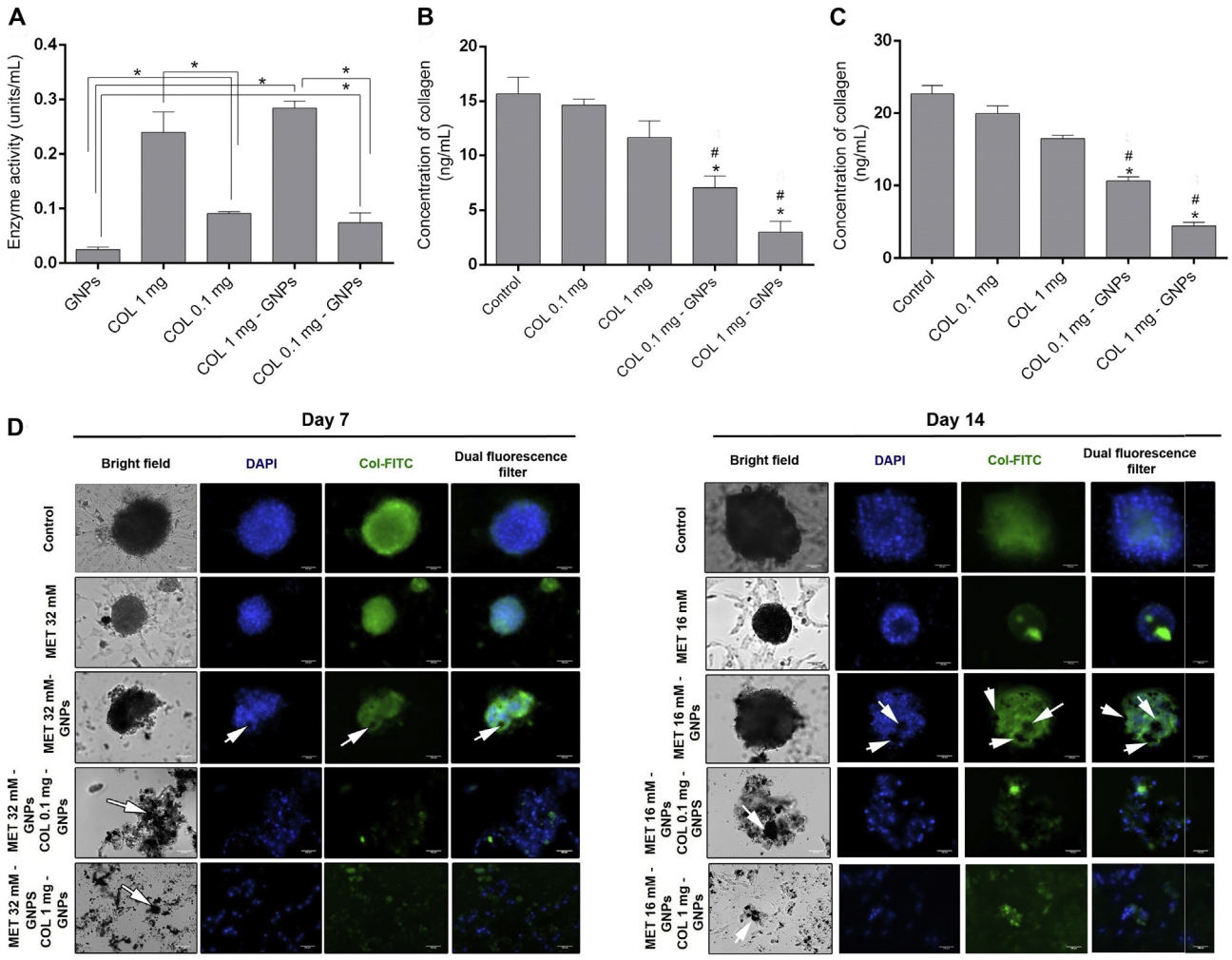

Fig. 2. Effects of collagenase (COL) on the collagen content in mammospheres. (A) ELISA analysis of the activity of COL alone and COL-GNPs on the degradation of collagen in spheroids. Panels B and C represent the effects of COL on the collagen contents in 7-day and 14-day old mammospheres, respectively. (D) Immunofluorescence analysis of collagen content in mammospheres. * and # represent statistically significant ($p < 0.05$) difference with the control and COL, respectively.

3.3. COL-GNPs impacts on collagen contents

To show whether collagenase activity exists in COL-GNPs complex, we used a colorimetric assay. Based on results obtained from the collagenase activity assay, the COL-GNPs showed enzyme activity equivalent to the free collagenase group at the same concentration as compared to GNPs alone (Fig. 2A, $p < 0.05$). Further, the data show that the incubation of mammospheres with 0.1 and 1 mg/mL Col-GNPs resulted in a significant decrease of collagen content inside 7- and 14-day mammosphere in a similar trend (Figs. 2B, C; $p < 0.05$). Following 5 days treatment of the spheroids, we found a 2- and a 5-fold decrease in the collagen content with 0.1 and 1 mg/mL collagenase as compared to groups treated with the free collagenase (Fig. 2B, C; $p < 0.05$).

3.4. COL-GNPs effects on the integrity of mammospheres

In order to verify the loose structure of JIMT-1 multicellular spheroids following the COL treatment, the mammospheres were stained with an antibody recognizing the collagens (i.e., I-V isoforms) and imaged by means of fluorescent microscopy. Based on the fluorescence visualization, the existence of collagen was approved in the context of control spheroids (Fig. 2D). The staining confirmed a significant reduction in the fluorescence intensity, indicating a decrease of collagen content in the multicellular spheroids after the exposure to the COL-GNPs with the same trend for both of 7- and 14-day old mammospheres (Fig. 2D). It seems that the spheroids treated with 1 mg/mL COL were completely decomposed and a single cell suspension generated. Due to the impacts of COL-contained NPs on spheroids, cells at the periphery were evidently detached. These data show that the direct effect(s) of COL in cooperation with GNPs and MET might abrogate the integrity of JIMT-1 cells' aggregates.

3.5. Toxicity of MET-GNPs and COL-GNPs in JIMT-1 mammosphere

In the current experiment, we found the IC_{50} of 8 mM for MET in the 2D culture on day 5 of culture. We also performed MTT assay on JIMT-1 cells on both 2D culture and 3D systems to evaluate the cytotoxicity effects of MET, MET-GNPs, and the mixture of MET-GNPs and COL-GNPs on JIMT-1 on day 7 and day 14 (Fig. 1S). Based on the data obtained from the MTT analysis, no significant difference was observed in the IC_{50}in 2D culture within different groups (Fig. 3A). In comparison to the cellviability from 2D culture, the IC_{50} was not achieved with the increasing concentration of MET from 8 to 320 mM in 14-day old mammospheres (Fig. 3B) and similar results were obtained for 7-day old mammospheres (data not shown). Based on our findings, about 20 to 30% reduction in the cell viability was observed after 5 days for 14-day old mammospheres.

On day 12 (i.e., after 5 days treatment of 7-day old spheroids), the

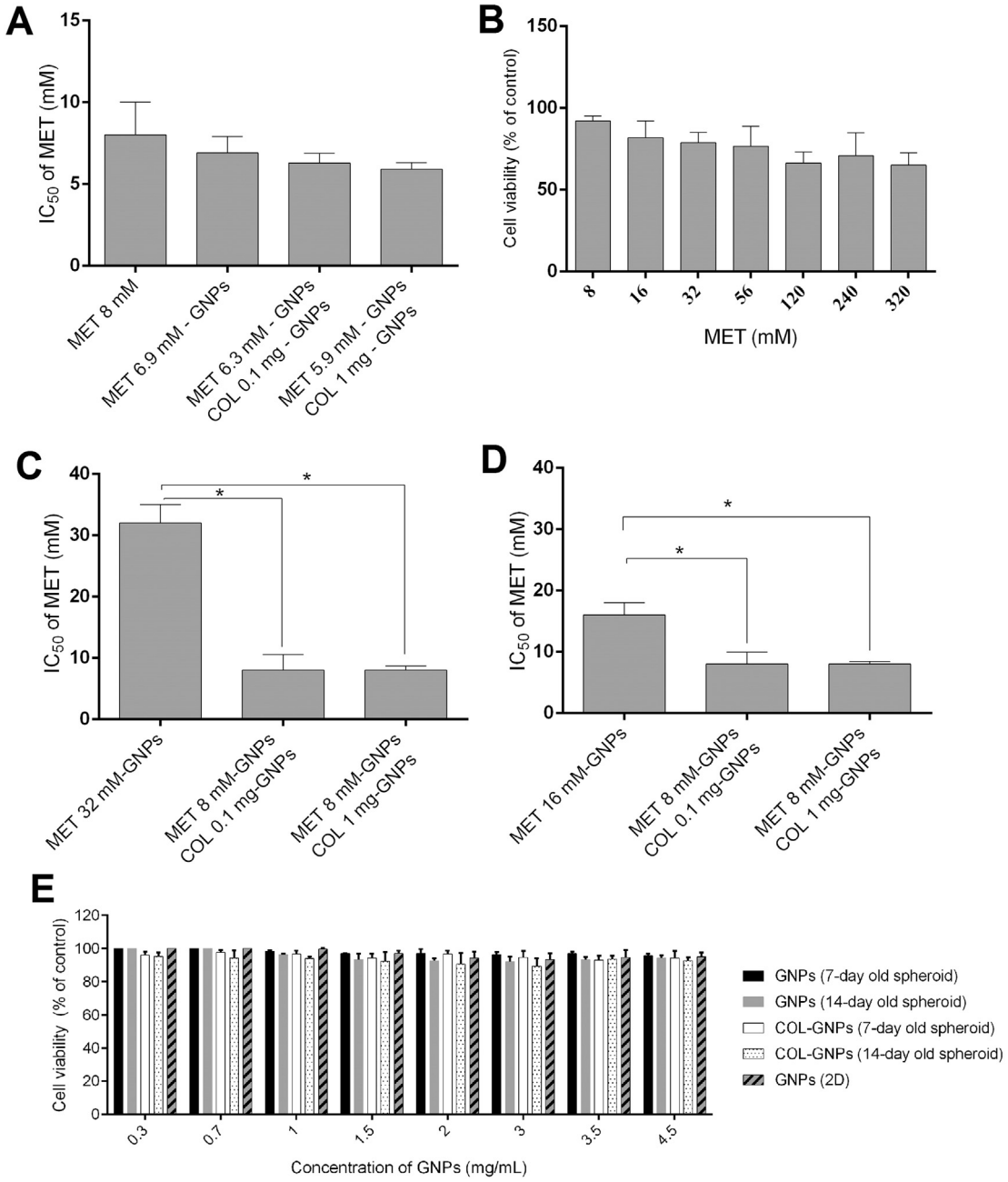

Fig. 3. The analysis of IC_{50} of treatments in the 2D and 3D cultures. (A) Comparison of the IC_{50} of treatments in each group in the 2D culture system. (B) The viability of JIMT-1 14 days old spheroids upon treatment with various concentrations of MET. (C) IC_{50} of MET in each group after 7 days. (D) IC_{50} of MET in each group after 14 days. (E) Effect of COL-GNPs and GNPs alone on the viability of cells in the 2D and 3D systems ($n = 3$). * represents statistically significant difference ($p < 0.05$).

IC_{50} of MET cells from mammosphere exposed to MET-GNPs was about 32 mM as compared to the mixture of the MET-GNPs and COL-GNPs (0.1 and 1 mg/mL) resulted in the IC_{50} of 8 mM. Notably, as shown in Fig. 3C, a 4-fold decrease was observed in the spheroids received the mixture of COL-GNPs and MET-GNPs as compared to MET-GNPs ($p < 0.05$). After 19 days (i.e., after 5 days treatment of 14-day old spheres) of the cultivation, the IC_{50} reached 16 mM in the MET-GNPs group, while this value was about 8 mM (2-fold lower) in the spheroids treated with the mixture of MET-GNPs and COL-GNPs ($p < 0.01$) (Fig. 3D).

Of note, higher cytotoxic activity was obtained in the mammospheres treated with the MET-GNPs after 19 days (MCRI of 2.3) and 12 days (MCRI of 4.6) compared to the 2D-culture system (Table 2). No differences were found in the cell cytotoxicity between 0.1 and 1 mg/

Table 2
IC_{50} and multicellular resistance index (MCRI) of culture evaluated for drug resistance.

Cell culture system	MET-GNPs		MET-GNPs COL (0.1 mg)-GNPs		MET-GNPs COL (1 mg)-GNPs	
	IC_{50} (mM)	MCR	IC_{50} (mM)	MCR	IC_{50} (mM)	MCR
2D culture	6.9 ± 1		6.3 ± 0.6		5.9 ± 0.4	
7-day old spheroids	32 ± 3	4.6	8 ± 2.5	1.2	8 ± 0.7	1.3
14-day old spheroids	16 ± 2	2.3	8 ± 1.94	1.2	8 ± 0.45	1.3

Table 3
$CD44^+/CD24^-$ population in JIMT-1 cells in 2D and 3D systems pre- and post-drug compound treatments.

Cell culture system	Control (%)	MET (%)	MET-GNPs (%)	MET-GNPs COL (0.1 mg)-GNPs (%)	MET-GNPs COL (1 mg)-GNPs (%)
2D culture	17 ± 1.1	10.69 ± 0.54*	10.27 ± 0.28*	9.32 ± 1.14*	8.95 ± 0.58*
7-day old spheroids	25.45 ± 0.84	15.76 ± 0.3	2.55 ± 0.47*	2.26 ± 0.38*	1.74 ± 0.27*
14-day old spheroids	37.86 ± 1.3	37.42 ± 0.54	11.41 ± 1.89*	11.29 ± 0.27*	7.87 ± 0.19*

* Statistical significance ($p < 0.05$) between control cells and treatment groups.

mL concentrations of COL and between the 2D and 3D (MCRI of 1.2). The COL-GNPs and GNPs in the 2D and 3D cultures showed no/trivial cytotoxic effects (Fig. 3E). Overall, we found that the tumoricidal effect of MET was decreased in the 3D culture. The application of COL and GNPs might synergize the detrimental effects of MET.

3.6. Inhibition of $CD44^+/CD24^-$ cells by MET-GNPs and COL-GNPs

The flow cytometry analysis revealed an increase in the percentage of the $CD44^+/CD24^-$ cells in the 3D culture system (reaching up to 25.45% and 37.86% in 7- and 14-day old mammospheres, respectively) as compared to the 2D culture with 17.1% CSCs (Fig. S2A; Table 3). These data support the notion that the population of the $CD44^+/CD24^-$ cells increased in spheroids in a time-dependent manner and reached the maximum level at day 14, indicating possible induction of CSCs-like phenotype. To examine the impacts of the treatments on the $CD44^+/CD24^-$ cells population, both 2D and 3D cultures were exposed to the different treatments of MET, MET-GNPs and the mixture of MET-GNPs and COL-GNPs. Based on our findings, a downward trend was found in the amount of CSCs in both 2D and 3D culture systems as compared to the untreated control cells ($p < 0.05$). In the 2D culture, statistically insignificant ($p > 0.05$) differences were found in the number of the $CD44^+/CD24^-$ cells in the groups treated with MET alone, MET-GNPs, and the mixture of MET-GNPs and COL-GNPs (Fig. 4A). In the 3D culture spheroids, MET had no significant ($p > 0.05$) effect compared to the untreated control (Fig. 4A). As expected, MET, in combination with GNPs and COL-GNPs, could significantly ($p < 0.05$) decrease the percentage of the $CD44^+/CD24^-$ cells compared to the control (Fig. 4A). On days 12 and 19 (i.e., 5 days treated 7- and 14-day old spheres), the most reduction in CSCs was indicated in the JIMT-1 cells treated with a mixture of COL-GNPs and MET-GNPs.

3.7. Induction of apoptosis in cells treated with MET-GNPs and COL-GNPs

The extent of apoptosis was evaluated by the flow cytometry analysis using FITC-labeled annexin-V/PI kit (Fig. S2B). Following the experimental procedure, the percent of early and late apoptotic cells was increased in the 2D and 3D cultures as compared to the control. In the 2D culture, no significant ($p > 0.05$) difference was found between the cells treated with MET alone and MET-GNPs. Further, no significant difference was found in the cells treated with the mixture of MET-GNPs and COL-GNPs between 0.1 and 1 mg COL, while the addition of COL made slight increase in the apoptosis (Fig. 4B). In the 3D culture, except for the cells treated with MET alone, we found significant ($p < 0.05$) increase in the number of apoptotic cells in the treated spheroids with MET-GNPs and the COL-GNPs and MET-GNPs mixture as compared to the untreated control after 12 and 19 days of cultivation (Fig. 4B). Notwithstanding, the addition of collagenase to MET-GNPs complex markedly ($p < 0.05$) increased the rate of apoptotic cells (i.e., both early and late apoptosis) up to 74 ± 5.5% on day 12 and 79 ± 9.4% on day 19 (Table 4). While we observed no cells entering the necrotic stages, the cells (in both the 2D and 3D systems) treated with the COL-GNPs and MET-GNPs mixture entered the late apoptosis stage, in which some population of cells appeared to show somewhat initial necrotic changes in the longer period of treatments.

3.8. Effect of MET-GNPs on PKM2 expression in mammospheres

To monitor the effect of the mixture of MET-GNPs and COL-GNPs on the tumor energetic pathway and lactate production, the transcription level of PKM2 was evaluated by the real-time PCR in both the 2D and 3D systems. Our findings showed that the MET-GNPs combined with COL-GNPs could significantly ($p < 0.05$) inhibit the expression of PKM2 as compared to untreated samples (Fig. 4C). In the 3D culture, it seems that MET alone or in combination with COL could slightly suppress the expression of PKM2, while such impact was significantly ($p < 0.05$) greater upon the treatment of the spheroids with the mixture of MET-GNPs and COL-GNPs (Fig. 4C). These data suggest that the inhibitory effect of MET was improved in the 3D system via simultaneous use of COL (either 0.1 or 1 mg/mL) and GNPs.

4. Discussion

Previous studies have demonstrated that cancer therapy using nanoparticle have limitation due to restricted drug penetration in tumor areas, in large part because of excessive rigidity of the ECM as a physical barrier to drug delivery [34,35]. It should be noted that the currently used anticancer therapeutics and even nanoscaled medicaments might fail to diffuse or penetrate into the hypoxic area of solid tumors where CSCs could remain untouched [37]. To tackle this limitation, solid tumors can be primed using ECM-modulating enzymes. In fact, the degradation of ECM, especially collagen network can be performed through COL enzyme as an effective and safe strategy to improve the tumor therapy [36]. However, there are several pitfalls in terms of the management of free COL molecules as adjuvant therapy, including undesired side effects of COL on healthy tissues. The use of COL-GNPs might moderate the degradation of localized ECM in solid tumors with minimal side effects imposed by the free COL.

Interestingly, some studies clarified that the cytotoxic effect of MET and breast cancer cells sensitivity might be increased under the hypoxic condition [38]. As a matter of fact, one could hypothesize that the MET tumoricidal effect could be mediated via modulation of the hypoxic area and imposing cytotoxic effects on the CSCs. This work investigates the penetration of MET-GNPs along with COL-GNPs in the 3D mammosphere as a more realistic model looking at the integrity changes in ECM. To the best of our knowledge, there are no reports regarding the combined use of MET-GNPs along with COL-GNPs in the 3D culture system, which highlight the importance of this current study.

In this study, the NPs were characterized using different techniques (Fig. 1), in which the sizes of NPs assessed by TEM analysis were somewhat smaller than those acquired by DLS, perhaps due to the two following reasons. First, the TEM analysis requires the dried NPs, while solvated NPs are used for DLS analysis. Second, the TEM analysis represents the number-average diameter, while the DLS examination demonstrates an intensity-weighted diameter [39,40].

Upon the conjugation of COL (0.1 and 1 mg/mL) onto GNPs, and treatment of the mamospheres, the collagen content was decreased approximately 2- and 5-fold as compared to that of the COL alone (Fig. 2). These results show that the use of COL-GNPs might result in an

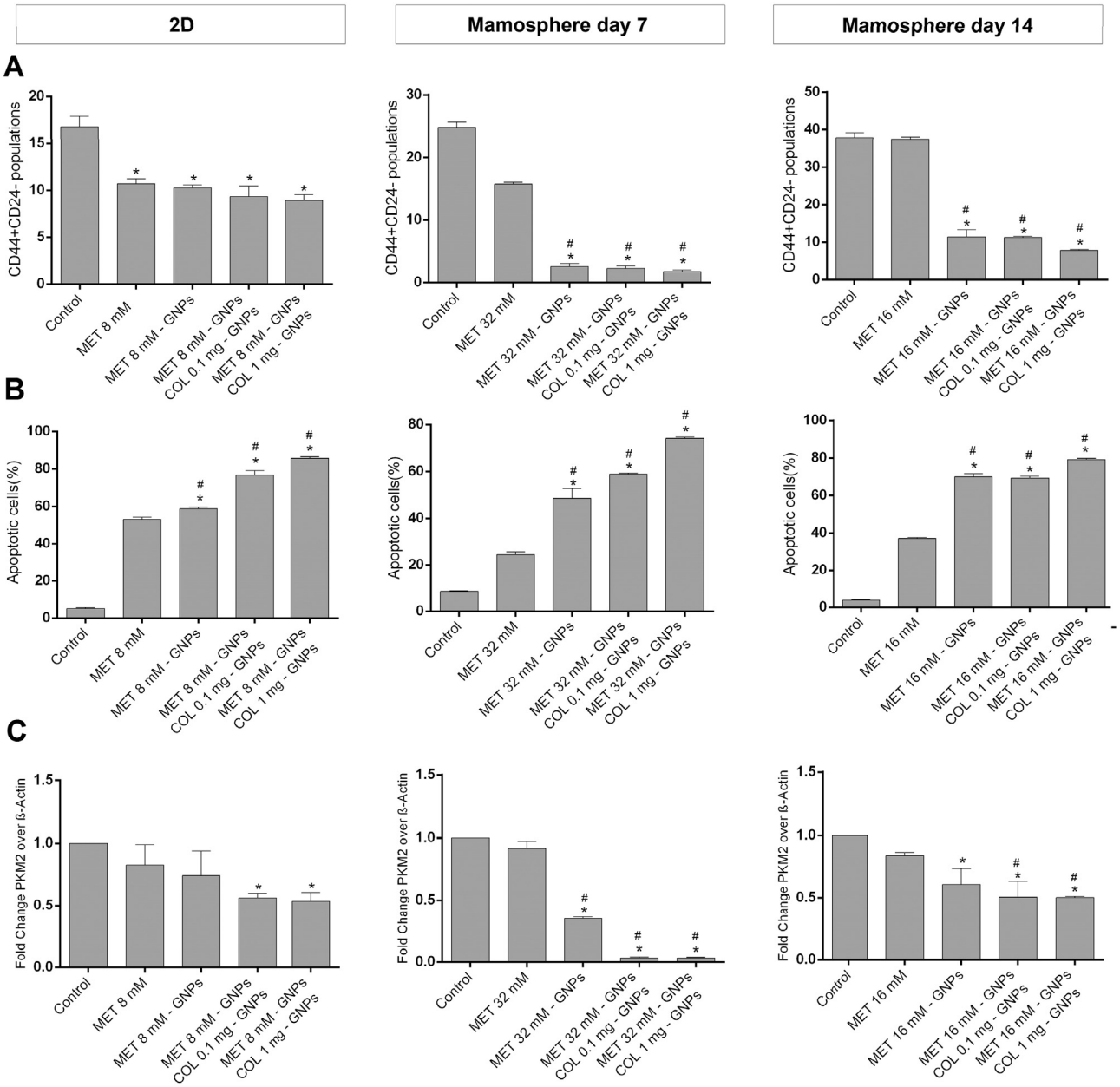

Fig. 4. Flow cytometry and real-time PCR analyses. (A) Flow cytometry of $CD44^{+}/CD24^{-}$ cells population in the 2D and 3D cultures of JIMT-1 cells before and after exposure to MET, MET-GNPs and the mixture of MET-GNPs and COL-GNPs after 7 and 14 days. (B) Analysis of apoptosis by annexin V/PI double-staining of JIMT-1 cells in the 2D and 3D system after 7 and 14 days. (C) PKM2 expression before and after treatments in the 2D and 3D cultures. * and # represent statistically significant ($p < 0.05$) difference with the control and MET, respectively.

Table 4
JIMT-1 cells entering apoptosis in 2D and 3D culture after 12 and 19 days of treatment with drug compounds.

Cell culture system	Apoptosis	Control (%)	MET (%)	MET-GNPs (%)	MET-GNPS COL 0.1 mg–GNPs (%)	MET-GNPs COL 1 mg–GNPs (%)
2D culture	Early	1.4 ± 0.15	30.2 ± 0.83*	24.08 ± 0.9*	21.5 ± 0.08*	17.9 ± 0.01*
	Late	3.55 ± 0.14	21.7 ± 0.42*	34.8 ± 0.3*	53.6 ± 1.6*	68.5 ± 0.82*
7-day old spheroids	Early	4.8 ± 0.001	21.2 ± 0.73*	35.8 ± 0.04*	31 ± 0.6*	41.9 ± 2.89*
	Late	3.7 ± 0.07	2.37 ± 0.06*	14.12 ± 0.4*	27.3 ± 0.07*	26.6 ± 2.7*
14-day old spheroids	Early	2.91 ± 0.02	36.8 ± 0.03*	58.8 ± 1.3*	46.4 ± 1.2*	56.2 ± 0.5*
	Late	0.91 ± 0.045	0.26 ± 0.004*	9.86 ± 0.01*	21.5 ± 0.3*	13.6 ± 8.9*

* Statistical significance ($p < 0.05$) between control cells and treatment groups.

enzymatic modulation of ECM in the inner area of the tumor mass, indicating improved delivery of COL to the inner core of the tumor. Therefore, the penetration of MET in the presence of COL is possibly facilitated to the cells located in the inner parts of spheroids, where CSCs are belived to reside.

The survival assay confirmed that MET could result in moderate cytotoxicity in JIMT-1 cells in the 2D cell culture system (Fig. 3), while this effect was relatively slight in the mammospheres, in large part because of lack of sufficient penetration of MET molecules into the tumor mass of the 3D culture. In fact, the cells located at the center of spheroids or juxtaposed to the sub-marginal region might be devoided the MET impacts. Commensurate with these findings, we observed that the cells at the periphery of spheroid were detached and subsequently undergone a cell death program. Besides, the penetration of MET-GNPs into the mammosphere was limited in the absence of COL treatment, in which most NPs remained concentrated at the spheroid edge. Based on our findings, due to an efficient drug penetration after the use of COL at doses 0.1 and 1 mg/mL, a decrease in IC_{50} of MET was found as compared to MET-GNPs (Table 2, Fig. 3). It seems that COL at a dose of 0.1 mg/mL might be suitable for the effectiveness of MET- GNPs treatment. We found a slight cell-to-cell disintegration at the outer spheroid surface during the treatment with 1 mg/mL of COL, which could abruptly decompose the spheroid structure [41]. It should be stated that the higher doses of COL were shown to efficiently affect the integrity of the mammospheres, resulting in further metastasis of untouched cancer cells and possible paraneoplastic phenomenon [42,43]. Such phenomena seem to be consistent with previous reports even though COL per se appears to be nontoxic to the cells [44]. In support of this claim, COL is believed to have no detrimental effects on the normal functions of cells, and hence, it has commonly been used for the detachment of cells. The result of the MCRI value showed that MCRI of the 7-day old spheroids was more than the 14-day old counterpart (Table 2). One explanation would be that the spheroids with a small diameter size have thin hypoxic layer compared to the large size mammospheres [45]. We also noticed a higher cytotoxic effect of MET-GNPs on the day 19 than that of the 12-day old 3D culture. In spite of higher collagen synthesis by the culture time (15.62 ± 1.52 ng at 12-day old spheroid versus 22.32 ± 1.15 at 19-day old spheroids), the cell survival was higher in the mammospheres after 12 days compared to spheroids on the day 19. Consistent with our result, Auvergne and colleagues reported that the treatment of the 7-and 14-day old human chondrosarcoma HEMC-SS cell spheroids with drug TH-302 imposed higher cytotoxicity in cells from day 14 [45]. This result is possibly related to the fact that the population of the hypoxic cells is increased after a prolonged culture period with a higher rate of sensitivity to MET [46]. The mechanism of the resistance seems to be an important factor in the efficiency of the anti-cancer agent [9]. Also, it was demonstrated the induction of collagen content by time, as confirmed in the current experiment, could markedly induce the expression of ECM degrading enzymes such as metalloproteinase, which may increase the penetration of MET-GNPs on the day 14 [47].

According to the great body of the experiment, $CD44^+/CD24^-$ are conceived as a biomarker for the identification of breast CSCs [48]. The latter phenomenon is speculated to emerge because of the functional presence of CSCs. Similar to other reports, our study showed the number of CSCs increased upon cultivation in the 3D condition [49]. The addition of COL to MET-GNPs complex could decrease the $CD44^+/CD24^-$ cell population in tumor mass, showing a gradual loss of stemness trait in the tumor foci (Table 3). This supports the possible reduction of CSCs that might decrease the tumor resistance to chemotherapeutic agents [50]. In support of this claim, the number of apoptotic cells was shown to increase after the treatment with GNPs conjugated with collagenase coincided with the downregulation of PKM2 (Fig. 4, Table 4). The decrease of PKM2 was shown to correlate with the cytotoxic effect of MET on the proliferation of cancer cells [51,52]. The reduction of PKM2 may limit the generation of ATP in cancer cells by inhibiting the transformation of phosphoenolpyruvate to pyruvate, and as a consequence, declining tumor growth [53]. Further, it should be stated that the lack of necrosis phenomena in our study might be related to the use of the immortalized cells that might possess trivial necrotic core in mammospheres [54]. As a result, we speculate that the longer incubation time with a much higher dose of MET-GNPs might lead some part of the cells in mammospheres to become necrotic, which demands further experimentations to be proven.

5. Conclusions

Mammospheres provide the 3D model systems, which can enrich the growth of rare cell types such as CSCs. Such models can be used for examining the therapeutic impact of compounds such as MET in cancer. Our findings support the role of ECM in terms of cancer cells' resistance to chemotherapeutic agents, which may result in the decline of drug efficacy and failure of cancer therapy. Taken all, it is proposed that the enzymatic modulation of ECM with collagenase-conjugated NPs (e.g., COL-GNPs) may enhance the penetration of chemotherapeutic agents and macroomolecules/NPs (e.g., MET-GNPs) into the solid tumor, and hence, result in improved therapeutic outcomes. Further, the use of gold NPs for the conjgation of collagenase may provide a great possibility for the phothermal therapy of solid tumors.

Declaration of Competing Interest

The authors declare no conflict of interest.

Acknowledgments

This study is part of a Ph.D. thesis and supported financially by Zanjan University of Medical Sciences (ID: A-12-892-11; Ethical Code: ZUMS.REC. 1395.42), the Cancer Control Research Center, Cancer Control Foundation, Iran University of Medical Sciences (ID: CCF-97067) and technically by the Research Center for Pharmaceutical Nanotechnology at Tabriz University of Medical Sciences.

Appendix A. Supplementary data

Supplementary data to this article can be found online at https://doi.org/10.1016/j.lfs.2019.116545.

References

[1] A. Kamb, What's wrong with our cancer models? Nat. Rev. Drug Discov. 4 (2005) 161–165.
[2] W.N. Hait, Anticancer drug development: the grand challenges, Nat. Rev. Drug Discov. 9 (2010) 253–254.
[3] C.J. Lovitt, et al., Advanced cell culture techniques for cancer drug discovery, Biology 3 (2014) 345–367.
[4] M. Vinci, et al., Advances in establishment and analysis of three-dimensional tumor spheroid-based functional assays for target validation and drug evaluation, BMC Biol. 10 (2012) 1741–7007.
[5] J. Barar, Y. Omidi, Dysregulated pH in tumor microenvironment checkmates cancer therapy, Bioimpacts 3 (2013) 149–162.
[6] Y. Omidi, J. Barar, Targeting tumor microenvironment: crossing tumor interstitial fluid by multifunctional nanomedicines, Bioimpacts 4 (2014) 55–67.
[7] D. Hanahan, R.A. Weinberg, The hallmarks of cancer, Cell 100 (2000) 57–70.
[8] M.R. Asgharzadeh, et al., Molecular machineries of pH dysregulation in tumor microenvironment: potential targets for cancer therapy, Bioimpacts 7 (2017) 115–133.
[9] M.R. Junttila, F.J. de Sauvage, Influence of tumour micro-environment heterogeneity on therapeutic response, Nature 501 (2013) 346–354.
[10] J.W. Ivey, et al., Improving cancer therapies by targeting the physical and chemical hallmarks of the tumor microenvironment, Cancer Lett. 380 (2016) 330–339.
[11] M. Eskandani, et al., Cell physiology regulation by hypoxia inducible factor-1: targeting oxygen-related nanomachineries of hypoxic cells, Int. J. Biol. Macromol. 99 (2017) 46–62.
[12] B. Viollet, et al., Cellular and molecular mechanisms of metformin: an overview, Clin. Sci. 122 (2012) 253–270.
[13] D.M. Nathan, et al., Medical management of hyperglycaemia in type 2 diabetes mellitus: a consensus algorithm for the initiation and adjustment of therapy: a

consensus statement from the American Diabetes Association and the European Association for the Study of Diabetes, Diabetologia 52 (2009) 17–30.
[14] V.N. Anisimov, et al., Effect of metformin on life span and on the development of spontaneous mammary tumors in her-2/neu transgenic mice, Exp. Gerontol. 40 (2005) 685–693.
[15] F. Feng, et al., Downregulation of rab27a contributes to metformin-induced suppression of breast cancer stem cells, Oncol. Lett. 14 (2017) 2947–2953.
[16] S. Mazurek, et al., Pyruvate kinase type m2 and its role in tumor growth and spreading, Semin. Cancer Biol. 15 (2005) 300–308.
[17] J.C. Tang, et al., Effects and mechanisms of metformin on the proliferation of esophageal cancer cells in vitro and in vivo, Cancer Res. Treat. 49 (2017) 778–789.
[18] A. Hamabe, et al., Role of pyruvate kinase m2 in transcriptional regulation leading to epithelial–mesenchymal transition, Proc. Natl. Acad. Sci. 111 (2014) 15526–15531.
[19] Y.-C. Yang, et al., Nuclear translocation of pkm2/ampk complex sustains cancer stem cell populations under glucose restriction stress, Cancer Lett. 421 (2018) 28–40.
[20] J. Lee, et al., Pyruvate kinase isozyme type m2 (pkm2) interacts and cooperates with oct-4 in regulating transcription, Int. J. Biochem. Cell Biol. 40 (2008) 1043–1054.
[21] W. Luo, et al., Pyruvate kinase m2 is a phd3-stimulated coactivator for hypoxia-inducible factor 1, cell 145 (2011) 732–744.
[22] P. Yang, et al., Pyruvate kinase m2 facilitates colon cancer cell migration via the modulation of stat3 signalling, Cell. Signal. 26 (2014) 1853–1862.
[23] W. Yang, et al., Nuclear pkm2 regulates β-catenin transactivation upon EGFR activation, Nature 480 (2011) 118.
[24] C.S. Kumar, et al., Hyaluronic acid co-functionalized gold nanoparticle complex for the targeted delivery of metformin in the treatment of liver cancer (hepg2 cells), Carbohydr. Polym. 128 (2015) 63–74.
[25] K.R. Levental, et al., Matrix crosslinking forces tumor progression by enhancing integrin signaling, Cell 139 (2009) 891–906.
[26] J.I. Lopez, et al., In situ force mapping of mammary gland transformation, Integr. Biol. 3 (2011) 910–921.
[27] S. Murty, et al., Nanoparticles functionalized with collagenase exhibit improved tumor accumulation in a murine xenograft model, Part. Part. Syst. Charact. 31 (2014) 1307–1312.
[28] P. Ghosh, et al., Gold nanoparticles in delivery applications, Adv. Drug Deliv. Rev. 60 (2008) 1307–1315.
[29] K. Froehlich, et al., Generation of multicellular breast cancer tumor spheroids: comparison of different protocols, J. Mammary Gland Biol. Neoplasia 21 (2016) 89–98.
[30] N. Zheng, et al., One-step one-phase synthesis of monodisperse noble-metallic nanoparticles and their colloidal crystals, J. Am. Chem. Soc. 128 (2006) 6550–6551.
[31] M. Fathi, et al., Thermo-sensitive chitosan copolymer-gold hybrid nanoparticles as a nanocarrier for delivery of erlotinib, Int. J. Biol. Macromol. 106 (2018) 266–276.
[32] M.W. Pfaffl, A new mathematical model for relative quantification in real-time rt–pcr, Nucleic Acids Res. 29 (2001) e45.
[33] R. Greenwood, Review of the measurement of zeta potentials in concentrated aqueous suspensions using electroacoustics, Adv. Colloid Interf. Sci. 106 (2003) 55–81.
[34] H.Y. Tanaka, M.R. Kano, Stromal barriers to nanomedicine penetration in the pancreatic tumor microenvironment, Cancer Sci. 109 (2018) 2085.
[35] L.T. Curtis, H.B. Frieboes, The tumor microenvironment as a barrier to cancer nanotherapy, Systems biology of tumor microenvironment (2016) 165–190.
[36] M.R. Villegas, et al., Hybrid collagenase nanocapsules for enhanced nanocarrier penetration in tumoral tissues, ACS Appl. Mater. Interfaces 7 (2015) 24075–24081.
[37] X. Zheng, et al., Doxorubicin fails to eradicate cancer stem cells derived from anaplastic thyroid carcinoma cells: characterization of resistant cells, Int. J. Oncol. 37 (2010) 307–315.
[38] X. Zhou, et al., Metformin suppresses hypoxia-induced stabilization of hif-1alpha through reprogramming of oxygen metabolism in hepatocellular carcinoma, Oncotarget 7 (2016) 873–884.
[39] F. Mahmoodzadeh, et al., A novel dual stimuli-responsive thiol-end-capped abc triblock copolymer: synthesis via reversible addition–fragmentation chain transfer technique, and investigation of its self-assembly behavior, Polym. Int. 66 (2017) 1651–1661.
[40] A. Ghamkhari, et al., Novel 'schizophrenic' diblock copolymer synthesized via raft polymerization: poly(2-succinyloxyethyl methacrylate)-b-poly[(n-4-vinylbenzyl),n,n-diethylamine], Des. Monomers Polym. 20 (2016) 190–200.
[41] T.T. Goodman, et al., Increased nanoparticle penetration in collagenase-treated multicellular spheroids, Int. J. Nanomedicine 2 (2007) 265–274.
[42] J.S. Blackburn, et al., Rna interference inhibition of matrix metalloproteinase-1 prevents melanoma metastasis by reducing tumor collagenase activity and angiogenesis, Cancer Res. 67 (2007) 10849–10858.
[43] W.G. Stetler-Stevenson, Type IV collagenases in tumor invasion and metastasis, Cancer Metastasis Rev. 9 (1990) 289–303.
[44] H. Chang, et al., Safety of adipose-derived stem cells and collagenase in fat tissue preparation, Aesthet. Plast. Surg. 37 (2013) 802–808.
[45] A. Voissiere, et al., Development and characterization of a human three-dimensional chondrosarcoma culture for in vitro drug testing, PLoS One 12 (2017) e0181340.
[46] A. Dhawan, et al., Mathematical modelling of phenotypic plasticity and conversion to a stem-cell state under hypoxia, Sci. Rep. 6 (2016) 18074.
[47] S.P. Carey, et al., Three-dimensional collagen matrix induces a mechanosensitive invasive epithelial phenotype, Sci. Rep. 7 (2017) 42088.
[48] F.F. de Beca, et al., Cancer stem cells markers cd44, cd24 and aldh1 in breast cancer special histological types, J. Clin. Pathol. 66 (2013) 187–191.
[49] Z.W. Zhu, et al., A novel three-dimensional tumorsphere culture system for the efficient and low-cost enrichment of cancer stem cells with natural polymers, Exp. Ther. Med. 15 (2018) 85–92.
[50] T. Tanei, et al., Association of breast cancer stem cells identified by aldehyde dehydrogenase 1 expression with resistance to sequential paclitaxel and epirubicin-based chemotherapy for breast cancers, Clin. Cancer Res. 15 (2009) 4234–4241.
[51] A. Silvestri, et al., Metformin induces apoptosis and downregulates pyruvate kinase m2 in breast cancer cells only when grown in nutrient-poor conditions, PLoS One 10 (2015) e0136250.
[52] G. Chen, et al., Metformin inhibits gastric cancer via the inhibition of hif1α/pkm2 signaling, Am. J. Cancer Res. 5 (2015) 1423.
[53] G. Dong, et al., Pkm2 and cancer: the function of pkm2 beyond glycolysis, Oncol. Lett. 11 (2016) 1980–1986.
[54] J. Friedrich, et al., Experimental anti-tumor therapy in 3-d: spheroids–old hat or new challenge? Int. J. Radiat. Biol. 83 (2007) 849–871.